Acta Cryst E CRYSTALLOGRAPHIC COMMUNICATIONS

ISSN 2056-9890

Structure of entinostat Form B, $C_{21}H_{20}N_4O_3$, derived using laboratory powder diffraction data and density functional techniques

James A. Kaduk[a]* and Sunil Kumar Rai[b]

[a]Department of Chemistry, North Central College, 131 S. Loomis, St., Naperville IL, 60540 , USA, and [b]Department of Chemistry, Faculty of Science, University of Lucknow, Lucknow 226007, Uttar Pradesh, India. *Correspondence e-mail: kaduk@polycrystallography.com

Received 24 July 2025
Accepted 18 August 2025

Edited by W. T. A. Harrison, University of Aberdeen, United Kingdom

Keywords: powder diffraction; entinostat; Rietveld refinement; density functional theory.

CCDC references: 2481225; 2481224

Supporting information: this article has supporting information at journals.iucr.org/e

The crystal structure of entinostat Form B, $C_{21}H_{20}N_4O_3$, has been solved and refined using laboratory X-ray powder diffraction data, and optimized using density functional techniques. Entinostat crystallizes in space group $Pna2_1$ and the crystal structure consists of interlocking layers of entinostat molecules parallel to the *bc* plane. A strong N—H···N hydrogen bond links the molecules into zigzag chains propagating along the *b*-axis direction. The graph set for this pattern is $C_1^1(8)$. Two N—H···O hydrogen bonds link the molecules along the *c*-axis direction. The graph sets for this pattern are $C_1^1(4)$ and $C_1^1(7)$.

1. Chemical context

Entinostat, $C_{21}H_{20}N_4O_3$ (also known as SNDX-275 and MS-275), is undergoing clinic trials for treatment of various cancers. The rights to entinostat are owned by Syndax Pharmaceuticals. The systematic name (CAS Registry No. 209783-80-2) is pyridin-3-ylmethyl *N*-({4-[(2-aminophenyl)carbamoyl]phenyl}methyl)carbamate.

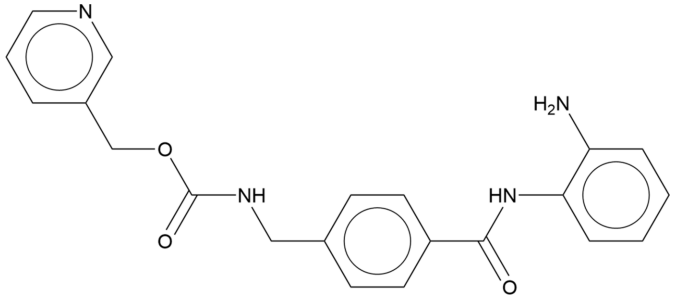

International Patent Application WO2010/022988 A1 (Schneider *et al.*, 2010; Bayer Schering Pharma) discloses crystalline Forms A, B, and C of entinostat and processes for their preparation. The material characterized here appears to be Form B (Fig. 1). Crystalline Forms D and E are disclosed in International Patent Application 2017/081278 A1 (Stefinovic & Reece, 2017; Sandoz AG). Stable amorphous entinostat is claimed in International Patent Application WO2017/216761 (Peddireddy *et al.*, 2017; Dr. Reddys Laboratories). Cocrystals of entinostat with maleic acid (Form A) and succinic acid (Forms A, B, and C) are claimed in US Patent Application US2024/023948 A1 (Bonnaud & Prentice, 2024; Macfarlan Smith Ltd.). This work was carried out as part of a project aimed at preparing cocrystals of active pharmaceutical ingredients using mechanochemical techniques.

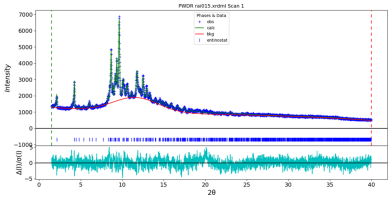

OPEN ACCESS
Published under a CC BY 4.0 licence

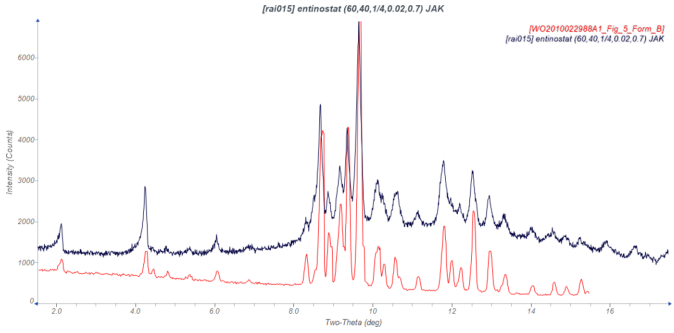

Figure 1
Comparison of the laboratory pattern of entinostat (measured using Mo K_α radiation; black) to that of Form B reported by Schneider *et al.* (2010; red). The patent pattern (measured using Cu K_α radiation) was digitized using *UN-SCAN-IT* (Silk Scientific, 2013) and converted to the Mo K_α wavelength of 0.7093187 Å using *JADE Pro* (MDI, 2025). Image generated using *JADE Pro* (MDI, 2025).

2. Structural commentary

The root-mean-square Cartesian displacement between the Rietveld-refined and VASP-optimized structures is 0.068 Å (Fig. 2). The agreement is within the normal range for correct structures (van de Streek & Neumann, 2014). The asymmetric unit of the structure is illustrated in Fig. 3. The remaining discussion will emphasize the VASP-optimized structure.

All of the bond distances, bond angles, and torsion angles fall within the normal ranges indicated by a *Mercury* Mogul geometry check (Macrae *et al.*, 2020). Quantum chemical geometry optimization of the isolated entinostat molecule (DFT/B3LYP/6-31G*/water) using *Spartan 24* (Wavefunction, 2023) indicated that the observed conformation is only 3.8 kcal mol^{-1} higher in energy than a local minimum, even though the r.m.s. displacement is 0.498 Å. The global minimum-energy conformation is much more compact (folded on itself to yield parallel phenyl rings), indicating that intermolecular interactions are important in determining the solid-state conformation. The false minimum structures contained different conformations of the molecule in roughly the same positions and orientation.

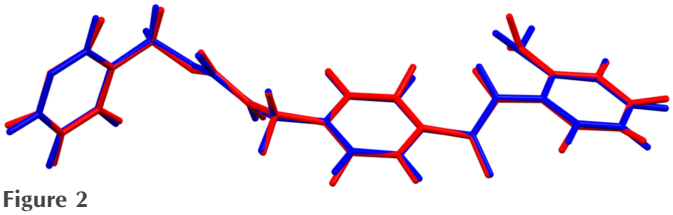

Figure 2
Comparison of the refined structure of the entinostat molecule (red) to the VASP-optimized structure (blue). The comparison was generated using the *Mercury* calculate/molecule overlay tool; the r.m.s. difference is 0.068 Å. Image generated using *Mercury* (Macrae *et al.*, 2020).

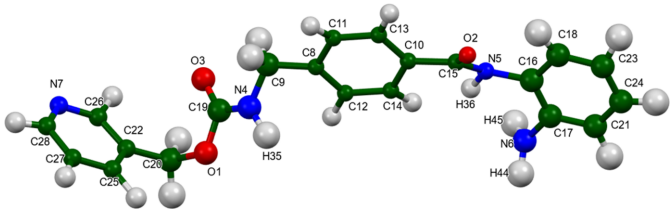

Figure 3
The asymmetric unit of entinostat Form B, with the atom numbering. The atoms are represented by 50% probability spheroids. Image generated using *Mercury* (Macrae *et al.*, 2020).

Table 1
Hydrogen-bond geometry (Å, °) for entinostat Form B.

D—H···A	D—H	H···A	D···A	D—H···A
N4—H35···N7^{i}	1.05	1.86	2.906	174
N5—H36···O2^{ii}	1.03	1.91	2.923	168
N6—H45···O2^{ii}	1.02	2.03	3.034	166
C9—H29···O3^{iii}	1.10	2.39	3.482	170
C25—H43···O3^{i}	1.09	2.33	3.281	144
C26—H46···O1^{iv}	1.09	2.34	3.199	135

Symmetry codes: (i) $-x+\frac{3}{2}, y-\frac{1}{2}, z-\frac{1}{2}$; (ii) $x, y, z+1$; (iii) $x, y, z-1$; (iv) $-x+\frac{3}{2}, y+\frac{1}{2}, z+\frac{1}{2}$.

3. Supramolecular features

The extended structure (Fig. 4) consists of interlocking layers of entinostat molecules lying parallel to the *bc* plane. Hydrogen bonds (discussed below) link the molecules along the *b*- and *c*-axis directions. The mean planes of the aminophenyl, phenyl, and pyridine rings correspond approximately to the (17,–5,–2), (13,–7,–3), and (26,–3,4) Miller planes, respectively. The *Mercury* aromatics analyser indicates strong interactions (centroid–centroid distance = 5.07 Å) between the two types of phenyl rings, moderate interactions with distances of 5.63 and 5.77 Å, as well as weaker interactions.

Analysis of the contributions to the total crystal energy of the structure using the Forcite module of *Materials Studio* (Dassault Systèmes, 2023) indicates that bond, angle, and torsion distortion terms contribute about equally to the intramolecular energy. The intermolecular energy is dominated by electrostatic attractions, which in this force field based analysis also include hydrogen bonds. The hydrogen bonds are better discussed using the results of the DFT calculation.

A strong N—H···N hydrogen bond links the molecules into zigzag chains along the *b*-axis direction (Table 1). The graph set (Etter, 1990; Bernstein *et al.*, 1995; Motherwell *et al.*, 2000) for this pattern is $C_1^1(8)$. Two N—H···O hydrogen bonds link the molecules along the *c*-axis direction. The graph sets for this pattern are $C_1^1(4)$ and $C_1^1(7)$. The energies of the N—H···O hydrogen bonds were calculated using the corre-

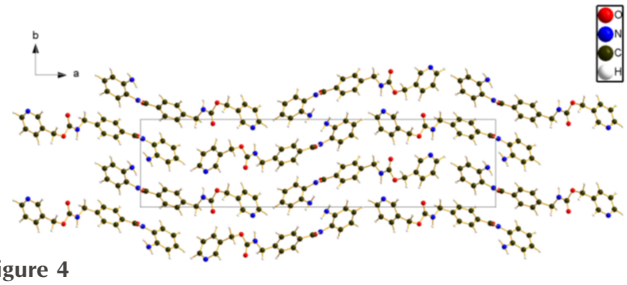

Figure 4
The crystal structure of entinostat Form B, viewed down the *c*-axis. Image generated using *DIAMOND* (Brandenburg & Putz, 2023).

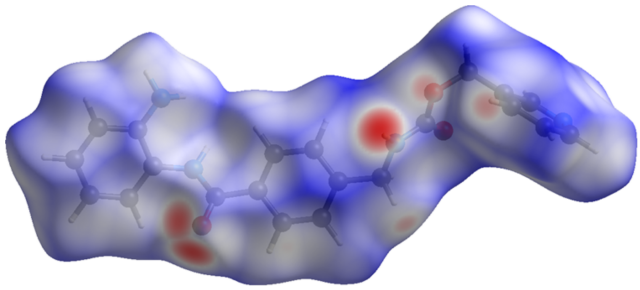

Figure 5
The Hirshfeld surface of entinostat Form B. Intermolecular contacts longer than the sums of the van der Waals radii are colored blue, and contacts shorter than the sums of the radii are colored red. Contacts equal to the sums of radii are white. Image generated using *CrystalExplorer* (Spackman *et al.*, 2021).

lation of Wheatley & Kaduk (2019). Several inter- and intramolecular C—H···O hydrogen bonds, as well as one C—H···N hydrogen bond, contribute to the lattice energy.

The volume enclosed by the Hirshfeld surface of entinostat (Fig. 5, Hirshfeld, 1977, Spackman *et al.*, 2021) is 448.9 Å^3 or 98.1% of 1/4 of the unit-cell volume. The packing density is thus fairly typical. The only significant close contacts (red in Fig. 5) involve the hydrogen bonds. The volume per non-hydrogen atom is smaller than normal, at 16.3 Å^3.

The Bravais–Friedel–Donnay–Harker (Bravais, 1866; Friedel, 1907; Donnay & Harker, 1937) algorithm suggests that we might expect platy morphology for entinostat, with {200} as the principal faces. A second order spherical harmonic model was included in the refinement. The texture index was 1.002 (1), indicating that preferred orientation was not significant in the rotated capillary specimen.

4. Database survey

A reduced cell search in the Cambridge Structural Database (CSD, version 2025.1.0 May 2025; Groom *et al.*, 2016) yielded 33 hits, but no structures for entinostat or its derivatives. A connectivity search of the entinostat molecule in the CSD yielded no hits. A search of the pattern against the Powder Diffraction File (Kabekkodu *et al.*, 2024) yielded no hits, and a name search on 'entinostat' also yielded no hits.

5. Synthesis and crystallization

The sample characterized here was obtained from a commercial source, was gently ground in a mortar and pestle and sieved to < 325 mesh.

6. Refinement

Crystal data, data collection and structure refinement details are summarized in Table 2. The pattern was indexed using *DICVOL14* (Louër & Boultif, 2014) on a primitive orthorhombic unit cell with a = 38.2913, b = 9.4545, c = 5.0779 Å, V = 1838.31 Å^3, and Z = 4.

The space group was ambiguous. Space groups $Pna2_1$, $Pca2_1$, $Pba2$, and $P2_12_12_1$ yielded similar profile fits, so the structure was solved in all of them using Monte Carlo-simulated annealing techniques as implemented in *FOX* (Favre-Nicolin & Černý, 2002) and/or *EXPO2014* (Altomare *et al.*, 2013). The entinostat molecule was downloaded from PubChem (Kim *et al.*, 2023) as Conformer3D_COMPOUND_CID_4261.sdf. It was converted to a *.mol2 file using *Mercury* (Macrae *et al.*, 2020), and to a Fenske-Hall Z-matrix using *OpenBabel* (O'Boyle *et al.*, 2011). The structures were optimized using *VASP* (Kresse & Furthmüller, 1996). Since space group $Pna2_1$ yielded the lowest energy, it was adopted for the final refinements and discussion.

Table 2
Experimental details.

	Rietveld
Crystal data	
Chemical formula	$C_{21}H_{20}N_4O_3$
M_r	376.42
Crystal system, space group	Orthorhombic, $Pna2_1$
Temperature (K)	300
a, b, c (Å)	38.236 (5), 9.4459 (7), 5.0673 (4)
V (Å^3)	1830.2 (2)
Z	4
Radiation type	Mo $K\alpha_{1,2}$, λ = 0.70932, 0.71361 Å
Specimen shape, size (mm)	Cylinder, 12 × 0.7
Data collection	
Diffractometer	PANalytical Empyrean
Specimen mounting	Glass capillary
Data collection mode	Transmission
Scan method	Step
2θ values (°)	$2\theta_{min}$ = 1.002 $2\theta_{max}$ = 49.991 $2\theta_{step}$ = 0.008
Refinement	
R factors and goodness of fit	R_p = 0.029, R_{wp} = 0.036, R_{exp} = 0.029, $R(F^2)$ = 0.11709, χ^2 = 1.636
No. of parameters	107
No. of restraints	72
H-atom treatment	Only H-atom displacement parameters refined
$(\Delta/\sigma)_{max}$	0.368

Computer programs: *FOX* (Favre-Nicolin & Černý, 2002) and *GSAS-II* (Toby & Von Dreele, 2013).

Several false minima were encountered during structure solution. There were three signs that these were not the correct structure, even though R_{wp} was as low as 0.0466: (1) the agreement of the Rietveld-refined and DFT-optimized structure was poor (root-mean-square Cartesian displacement ~0.9 Å – outside the normal range for correct structures); (2) the DFT optimization was very slow to converge (> 600 cycles of geometry optimization); (3) the displacement coefficients were much larger than expected (> 0.2 Å^2). To overcome these false minima, additional cycles (183) of parallel tempering in *FOX* were carried out to yield the structure described here.

Rietveld refinement was carried out with *GSAS-II* (Toby & Von Dreele, 2013). Only the 1.5–40.0° portion of the pattern was included in the refinements (d_{min} = 1.037 Å). All non-H bond distances and angles were subjected to restraints, based on a *Mercury*/Mogul geometry check (Sykes *et al.*, 2011; Bruno *et al.*, 2004). The Mogul average and standard deviation for each quantity were used as the restraint parameters. The three

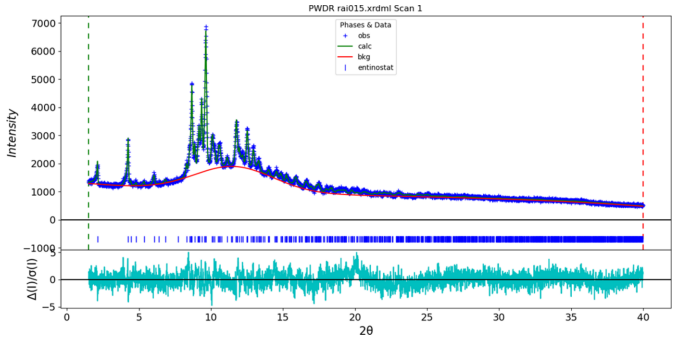

Figure 6
The Rietveld plot for entinostat Form B. The blue crosses represent the observed data points, and the green line is the calculated pattern. The cyan curve is the normalized error plot, and the red line is the background curve. The blue tick marks indicate the peak positions.

aromatic rings were restrained to be planar. The restraints contributed 3.2% to the overall χ^2. The hydrogen atoms were included in calculated positions, which were recalculated during the refinement using *Materials Studio* (Dassault Systèmes, 2023). The U_{iso} of the heavy atoms were grouped by chemical similarity. The U_{iso} for the H atoms were fixed at 1.3× the U_{iso} of the heavy atoms to which they are attached. The peak profiles were described using the generalized microstrain model (Stephens, 1999). The background was modeled using a four-term shifted Chebyshev polynomial, with a peak at 11.61° to model the scattering from the glass capillary. The final refinement of 107 variables using 4608 observations and 72 restraints yielded the residuals R_{wp} = 0.0697 and GOF = 1.28. The largest peak (0.19 Å from N7) and hole (1.46 Å from C10) in the difference-Fourier map are 0.61 (12) and −0.53 (12) e Å^{-3}, respectively. The final Rietveld plot is shown in Fig. 6. The largest features in the normalized error plot are in the intensities of some of the peaks.

The crystal structure of entinostat was optimized (fixed experimental unit cell) with density functional techniques using *VASP* (Kresse & Furthmüller, 1996) through the *MedeA* graphical interface (Materials Design, 2024). The calculation was carried out on 32 cores of a 144-core (768 Gb memory) HPE Superdome Flex 280 Linux server at North Central College. The calculation used the GGA-PBE functional, a plane wave cutoff energy of 400.0 eV, and a *k*-point spacing of 0.5 Å^{-1} leading to a 1 × 2 × 3 mesh, and took ∼4.2 h. Single-point density functional calculations (fixed experimental cell) and population analysis were carried out using *CRYSTAL23* (Erba *et al.*, 2023). The basis sets for the H, C, N and O atoms in the calculation were those of Gatti *et al.* (1994). The calculations were run on a 3.5 GHz PC using 8 k-points and the B3LYP functional, and took ∼2.4 h.

Acknowledgements

SKR thanks the University of Lucknow for providing research infrastructure.

Funding information

Funding for this research was provided by: SERB-ANRF New Delhi India (grant No. SUB/2022/002726).

References

Altomare, A., Cuocci, C., Giacovazzo, C., Moliterni, A., Rizzi, R., Corriero, N. & Falcicchio, A. (2013). *J. Appl. Cryst.* **46**, 1231–1235.
Bernstein, J., Davis, R. E., Shimoni, L. & Chang, N. L. (1995). *Angew. Chem. Int. Ed. Engl.* **34**, 1555–1573.
Bonnaud, T. & Prentice, Z. (2024). United States Patent Application US2024/023748 A1.
Brandenburg, K. & Putz, H. (2023). *DIAMOND*. Crystal Impact GbR, Bonn, Germany.
Bravais, A. (1866). *Etudes Cristallographiques*. Paris: Gauthier Villars.
Bruno, I. J., Cole, J. C., Kessler, M., Luo, J., Motherwell, W. D. S., Purkis, L. H., Smith, B. R., Taylor, R., Cooper, R. I., Harris, S. E. & Orpen, A. G. (2004). *J. Chem. Inf. Comput. Sci.* **44**, 2133–2144.
Dassault Systèmes (2023). *Materials Studio 2024*. BIOVIA, San Diego, CA, USA.
Donnay, J. D. H. & Harker, D. (1937). *Am. Mineral.* **22**, 446–447.
Erba, A., Desmarais, J. K., Casassa, S., Civalleri, B., Donà, L., Bush, I. J., Searle, B., Maschio, L., Edith-Daga, L., Cossard, A., Ribaldone, C., Ascrizzi, E., Marana, N. L., Flament, J.-P. & Kirtman, B. (2023). *J. Chem. Theory Comput.* **19**, 6891–6932.
Etter, M. C. (1990). *Acc. Chem. Res.* **23**, 120–126.
Favre-Nicolin, V. & Černý, R. (2002). *J. Appl. Cryst.* **35**, 734–743.
Friedel, G. (1907). *Bull. Soc. Fr. Mineral.* **30**, 326–455.
Gatti, C., Saunders, V. R. & Roetti, C. (1994). *J. Chem. Phys.* **101**, 10686–10696.
Groom, C. R., Bruno, I. J., Lightfoot, M. P. & Ward, S. C. (2016). *Acta Cryst.* B**72**, 171–179.
Hirshfeld, F. L. (1977). *Theor. Chem. Acta* **44**, 129–138.
Kabekkodu, S., Dosen, A. & Blanton, T. N. (2024). *Powder Diffr.* **39**, 47–59.
Kresse, G. & Furthmüller, J. (1996). *Comput. Mater. Sci.* **6**, 15–50.
Kim, S., Chen, J., Cheng, T., Gindulyte, A., He, J., He, S., Li, Q., Shoemaker, B. A., Thiessen, P. A., Yu, B., Zaslavsky, L., Zhang, J. & Bolton, E. E. (2023). *Nucleic Acids Res.* **51**(D1), D1373–D1380. https://doi.org/10.1093/nar/gkac956.
Louër, D. & Boultif, A. (2014). *Powder Diffr.* **29**, S7–S12.
Macrae, C. F., Sovago, I., Cottrell, S. J., Galek, P. T. A., McCabe, P., Pidcock, E., Platings, M., Shields, G. P., Stevens, J. S., Towler, M. & Wood, P. A. (2020). *J. Appl. Cryst.* **53**, 226–235.
Materials Design. (2024). *MedeA 3.7.2*. Materials Design Inc., San Diego, CA, USA.
MDI. (2025). *JADE Pro 9.3*. Materials Data, Livermore, CA, USA.
Motherwell, W. D. S., Shields, G. P. & Allen, F. H. (2000). *Acta Cryst.* B**56**, 857–871.
O'Boyle, N. M., Banck, M., James, C. A., Morley, C., Vandermeersch, T. & Hutchison, G. R. (2011). *J. Chem. Informatics* **3**, 33. https://doi.org/10.1186/1758-2946-3-33.
Peddireddy, S. R., Allam, S. K., Jurupula, R., Oruganti, S., Kandagatla, B., Dahanukar, V. H. & Peddy, V. (2017). International Patent Application WO2017/216761.
Schneider, M., Gottfried, M., Geisler, J. & Winter, G. (2010). International Patent Application WO2010/022988.
Silk Scientific (2013). *UN-SCAN-IT 7.0*. Silk Scientific Corporation, Orem, UT, USA.
Spackman, P. R., Turner, M. J., McKinnon, J. J., Wolff, S. K., Grimwood, D. J., Jayatilaka, D. & Spackman, M. A. (2021). *J. Appl. Cryst.* **54**, 1006–1011.
Stefinovic, M. & Reece, H. (2017). International Patent Application WO2017/081278 A1.

Stephens, P. W. (1999). *J. Appl. Cryst.* **32**, 281–289.
Streek, J. van de & Neumann, M. A. (2014). *Acta Cryst.* B**70**, 1020–1032.
Sykes, R. A., McCabe, P., Allen, F. H., Battle, G. M., Bruno, I. J. & Wood, P. A. (2011). *J. Appl. Cryst.* **44**, 882–886.
Toby, B. H. & Von Dreele, R. B. (2013). *J. Appl. Cryst.* **46**, 544–549.
Wavefunction (2023). *Spartan 24. V. 1.0.*0. Wavefunction Inc., Irvine CA, USA.
Wheatley, A. M. & Kaduk, J. A. (2019). *Powder Diffr.* **34**, 35–43.

supporting information

Acta Cryst. (2025). E**81**, 865-869 [https://doi.org/10.1107/S2056989025007406]

Structure of entinostat Form B, $C_{21}H_{20}N_4O_3$, derived using laboratory powder diffraction data and density functional techniques

James A. Kaduk and Sunil Kumar Rai

Computing details

Pyridin-3-ylmethyl *N*-({4-[(2-aminophenyl)carbamoyl]phenyl}methyl)carbamate (Rietveld)

Crystal data

$C_{21}H_{20}N_4O_3$
M_r = 376.42
Orthorhombic, $Pna2_1$
a = 38.236 (5) Å
b = 9.4459 (7) Å
c = 5.0673 (4) Å
V = 1830.2 (2) Å^3
Z = 4
D_x = 1.366 Mg m^{-3}
Mo $K\alpha_{1,2}$ radiation, λ = 0.70932, 0.71361 Å
T = 300 K
cylinder, 12 × 0.7 mm

Data collection

PANalytical Empyrean diffractometer
Radiation source: sealed X-ray tube
Zr filter monochromator
Specimen mounting: glass capillary
Data collection mode: transmission
Scan method: step
$2\theta_{min}$ = 1.002°, $2\theta_{max}$ = 49.991°, $2\theta_{step}$ = 0.008°

Refinement

Least-squares matrix: full
R_p = 0.029
R_{wp} = 0.036
R_{exp} = 0.029
$R(F^2)$ = 0.11709
5864 data points
Profile function: Finger-Cox-Jephcoat function parameters U, V, W, X, Y, SH/L: peak variance(Gauss) = Utan(Th)^2+Vtan(Th)+W: peak HW(Lorentz) = X/cos(Th)+Ytan(Th); SH/L = S/L+H/L U, V, W in (centideg)^2, X & Y in centideg 25.531, 9.905, 0.000, 1.091, 3.951, 0.034,
107 parameters
72 restraints
23 constraints
Only H-atom displacement parameters refined
Weighting scheme based on measured s.u.'s
$(\Delta/\sigma)_{max}$ = 0.368
Background function: Background function: "chebyschev-1" function with 4 terms: 871.1(20), -360.1(18), 11.3(15), -45.5(16), Background peak parameters: pos, int, sig, gam: 11.611(13), 6.24(5)e5, 7.58(9)e4, 0.100,
Preferred orientation correction: Simple spherical harmonic correction Order = 2 Coefficients: 0:0:C(2,0) = 0.103(29); 0:0:C(2,2) = -0.018(21)

Fractional atomic coordinates and isotropic or equivalent isotropic displacement parameters (Å^2)

	x	*y*	*z*	U_{iso}*/U_{eq}
O1	0.7170 (5)	0.3108 (13)	1.26983	0.055 (8)*
O2	0.5094 (5)	0.313 (3)	0.331 (4)	0.029 (9)*
O3	0.7017 (6)	0.5418 (13)	1.292 (8)	0.055 (8)*

N4	0.6773 (5)	0.393 (2)	0.994 (5)	0.055 (8)*
N5	0.4935 (5)	0.278 (3)	0.760 (5)	0.029 (9)*
N6	0.4756 (7)	0.052 (3)	1.089 (7)	0.055 (10)*
N7	0.8163 (6)	0.5927 (17)	1.337 (8)	0.033 (9)*
C8	0.6206 (3)	0.4434 (17)	0.780 (5)	0.027 (8)*
C9	0.6556 (6)	0.500 (2)	0.869 (8)	0.055 (8)*
C10	0.5512 (3)	0.3708 (19)	0.659 (5)	0.027 (8)*
C11	0.6038 (4)	0.502 (3)	0.563 (5)	0.027 (8)*
C12	0.6023 (5)	0.347 (4)	0.933 (6)	0.027 (8)*
C13	0.5696 (3)	0.467 (2)	0.504 (5)	0.027 (8)*
C14	0.5681 (5)	0.311 (3)	0.875 (6)	0.027 (8)*
C15	0.5163 (4)	0.318 (3)	0.568 (4)	0.029 (9)*
C16	0.4613 (4)	0.207 (2)	0.725 (6)	0.055 (10)*
C17	0.4533 (7)	0.091 (3)	0.889 (8)	0.055 (10)*
C18	0.4383 (9)	0.246 (4)	0.523 (9)	0.055 (10)*
C19	0.6981 (5)	0.4247 (11)	1.198 (5)	0.055 (8)*
C20	0.7430 (4)	0.335 (2)	1.474 (4)	0.055 (8)*
C21	0.4222 (8)	0.017 (3)	0.844 (9)	0.055 (10)*
C22	0.7750 (5)	0.4006 (19)	1.352 (8)	0.033 (9)*
C23	0.4077 (7)	0.169 (4)	0.483 (8)	0.055 (10)*
C24	0.3997 (8)	0.056 (4)	0.643 (8)	0.055 (10)*
C25	0.7929 (8)	0.335 (3)	1.149 (7)	0.033 (9)*
C26	0.7880 (8)	0.529 (2)	1.439 (7)	0.033 (9)*
C27	0.8221 (8)	0.398 (3)	1.040 (9)	0.033 (9)*
C28	0.8329 (6)	0.526 (2)	1.140 (7)	0.033 (9)*
H29	0.67008	0.54448	0.69050	0.0713*
H30	0.65046	0.58991	1.01441	0.0713*
H31	0.62060	0.54691	0.39817	0.0356*
H32	0.61567	0.29902	1.10662	0.0356*
H33	0.55888	0.51030	0.32747	0.0356*
H34	0.55238	0.26635	1.04151	0.0356*
H35	0.67159	0.28737	0.92867	0.0713*
H36	0.50674	0.20423	0.89818	0.0372*
H37	0.45017	0.32241	0.38325	0.0721*
H38	0.74850	0.23110	1.55041	0.0713*
H39	0.73009	0.39869	1.62195	0.0713*
H40	0.41682	−0.08211	0.94296	0.0721*
H41	0.39034	0.23483	0.36479	0.0721*
H42	0.37377	0.02234	0.63785	0.0721*
H43	0.78356	0.22806	1.07112	0.0432*
H44	0.47309	−0.06399	1.12476	0.0721*
H45	0.46876	0.11006	1.27176	0.0721*
H46	0.77066	0.58946	1.57984	0.0432*
H47	0.83386	0.33515	0.89816	0.0432*
H48	0.85627	0.56225	1.10069	0.0432*

Geometric parameters (Å, º)

O1—C19	1.345 (3)	C19—O3	1.213 (2)
O1—C20	1.453 (3)	C19—N4	1.337 (3)
O2—C15	1.229 (3)	C20—O1	1.453 (3)
O3—C19	1.213 (2)	C20—C22	1.503 (3)
N4—C9	1.454 (2)	C20—H38	1.076 (19)
N4—C19	1.337 (3)	C20—H39	1.08 (2)
N4—H35	1.08 (2)	C21—C17	1.399 (3)
N5—C15	1.361 (4)	C21—C24	1.383 (2)
N5—C16	1.416 (3)	C21—H40	1.081 (19)
N5—H36	1.11 (3)	C22—C20	1.503 (3)
N6—C17	1.376 (4)	C22—C25	1.382 (3)
N6—H44	1.11 (2)	C22—C26	1.382 (3)
N6—H45	1.11 (4)	C23—C18	1.387 (2)
N7—C26	1.342 (3)	C23—C24	1.376 (3)
N7—C28	1.340 (3)	C23—H41	1.09 (3)
C8—C9	1.511 (3)	C24—C21	1.383 (2)
C8—C11	1.386 (2)	C24—C23	1.376 (3)
C8—C12	1.386 (2)	C24—H42	1.042 (19)
C9—N4	1.454 (2)	C25—C22	1.382 (3)
C9—C8	1.511 (3)	C25—C27	1.382 (2)
C9—H29	1.14 (4)	C25—H43	1.140 (15)
C9—H30	1.14 (4)	C26—N7	1.342 (3)
C10—C13	1.389 (2)	C26—C22	1.382 (3)
C10—C14	1.390 (2)	C26—H46	1.13 (3)
C10—C15	1.498 (3)	C27—C25	1.382 (2)
C11—C8	1.386 (2)	C27—C28	1.373 (3)
C11—C13	1.384 (2)	C27—H47	1.04 (3)
C11—H31	1.14 (2)	C28—N7	1.340 (3)
C12—C8	1.386 (2)	C28—C27	1.373 (3)
C12—C14	1.385 (2)	C28—H48	0.977 (17)
C12—H32	1.110 (17)	H29—C9	1.14 (4)
C13—C10	1.389 (2)	H30—C9	1.14 (4)
C13—C11	1.384 (2)	H31—C11	1.14 (2)
C13—H33	1.065 (18)	H32—C12	1.110 (17)
C14—C10	1.390 (2)	H33—C13	1.065 (18)
C14—C12	1.385 (2)	H34—C14	1.12 (2)
C14—H34	1.12 (2)	H35—N4	1.08 (2)
C15—O2	1.229 (3)	H36—N5	1.11 (3)
C15—N5	1.361 (4)	H37—C18	1.11 (3)
C15—C10	1.498 (3)	H38—C20	1.076 (19)
C16—N5	1.416 (3)	H39—C20	1.08 (2)
C16—C17	1.4050 (16)	H40—C21	1.081 (19)
C16—C18	1.395 (2)	H41—C23	1.09 (3)
C17—N6	1.376 (4)	H42—C24	1.042 (19)
C17—C16	1.4050 (16)	H43—C25	1.140 (15)
C17—C21	1.399 (3)	H44—N6	1.11 (2)

C18—C16	1.395 (2)	H45—N6	1.11 (4)
C18—C23	1.387 (2)	H46—C26	1.13 (3)
C18—H37	1.11 (3)	H47—C27	1.04 (3)
C19—O1	1.345 (3)	H48—C28	0.977 (17)
C19—O1—C20	115.7 (3)	C17—C16—C18	120.10 (11)
C9—N4—C19	121.6 (3)	N6—C17—C16	120.91 (14)
C9—N4—H35	113.2 (7)	N6—C17—C21	120.61 (15)
C19—N4—H35	124.4 (12)	C16—C17—C21	118.48 (10)
C15—N5—C16	126.8 (3)	C16—C18—C23	119.96 (16)
C15—N5—H36	109.5 (16)	C16—C18—H37	112.5 (17)
C16—N5—H36	100.2 (10)	C23—C18—H37	126.2 (18)
C17—N6—H44	109 (4)	O1—C19—O3	124.2 (2)
C17—N6—H45	109 (3)	O1—C19—N4	110.5 (2)
H44—N6—H45	109 (3)	O3—C19—N4	125.00 (19)
C26—N7—C28	117.34 (18)	O1—C20—C22	109.4 (3)
C9—C8—C11	120.4 (3)	O1—C20—H38	104.3 (11)
C9—C8—C12	120.7 (3)	C22—C20—H38	111.5 (18)
C11—C8—C12	118.22 (13)	O1—C20—H39	105.5 (9)
N4—C9—C8	113.0 (3)	C22—C20—H39	115.3 (14)
N4—C9—H29	109 (3)	H38—C20—H39	110.2 (17)
C8—C9—H29	108.9 (15)	C17—C21—C24	120.91 (13)
N4—C9—H30	109.5 (15)	C17—C21—H40	121 (2)
C8—C9—H30	108 (3)	C24—C21—H40	117 (3)
H29—C9—H30	108.9 (14)	C20—C22—C25	121.4 (2)
C13—C10—C14	118.34 (12)	C20—C22—C26	121.5 (2)
C13—C10—C15	119.6 (3)	C25—C22—C26	117.08 (14)
C14—C10—C15	121.4 (3)	C18—C23—C24	120.38 (13)
C8—C11—C13	121.06 (13)	C18—C23—H41	108 (2)
C8—C11—H31	118.0 (13)	C24—C23—H41	129 (3)
C13—C11—H31	117.6 (12)	C21—C24—C23	120.16 (12)
C8—C12—C14	120.99 (13)	C21—C24—H42	122 (3)
C8—C12—H32	118.7 (11)	C23—C24—H42	116 (3)
C14—C12—H32	120.3 (11)	C22—C25—C27	120.07 (15)
C10—C13—C11	120.70 (12)	C22—C25—H43	120.0 (11)
C10—C13—H33	122.3 (9)	C27—C25—H43	119.8 (13)
C11—C13—H33	116.9 (9)	N7—C26—C22	123.98 (18)
C10—C14—C12	120.69 (12)	N7—C26—H46	119.3 (15)
C10—C14—H34	119.9 (13)	C22—C26—H46	115.8 (14)
C12—C14—H34	115.9 (18)	C25—C27—C28	118.54 (16)
O2—C15—N5	123.4 (3)	C25—C27—H47	112.3 (15)
O2—C15—C10	120.3 (2)	C28—C27—H47	129.0 (15)
N5—C15—C10	116.3 (2)	N7—C28—C27	123.0 (2)
N5—C16—C17	118.9 (2)	N7—C28—H48	115 (2)
N5—C16—C18	121.0 (2)	C27—C28—H48	121 (2)

(VASP)

Crystal data

$C_{21}H_{20}N_4O_3$	b = 9.44590 Å
M_r = 376.42	c = 5.06730 Å
Orthorhombic, $Pna2_1$	V = 1830.17 Å^3
a = 38.23600 Å	Z = 4

Data collection

DFT optimization	$k = \rightarrow$
$h = \rightarrow$	$l = \rightarrow$

Fractional atomic coordinates and isotropic or equivalent isotropic displacement parameters (Å^2)

	x	y	z	B_{iso}*/B_{eq}
O1	0.71602	0.30908	1.29383	
O2	0.50809	0.30967	0.33129	
O3	0.70419	0.54791	1.27319	
N4	0.67730	0.38675	0.99681	
N5	0.49333	0.28080	0.76790	
N6	0.47635	0.04721	1.08292	
N7	0.81620	0.59379	1.32902	
C8	0.62069	0.44093	0.78248	
C9	0.65707	0.49049	0.85136	
C10	0.55157	0.36158	0.65553	
C11	0.60342	0.50113	0.56549	
C12	0.60305	0.33908	0.93232	
C13	0.56950	0.46114	0.50143	
C14	0.56879	0.30057	0.87182	
C15	0.51586	0.31652	0.57107	
C16	0.46077	0.21116	0.73033	
C17	0.45309	0.09247	0.89166	
C18	0.43725	0.25439	0.53534	
C19	0.69932	0.42603	1.19110	
C20	0.74344	0.33754	1.48371	
C21	0.42225	0.01638	0.83831	
C22	0.77550	0.39878	1.35610	
C23	0.40654	0.17878	0.48894	
C24	0.39948	0.05794	0.63863	
C25	0.79359	0.32785	1.15597	
C26	0.78808	0.53075	1.43545	
C27	0.82290	0.39187	1.04445	
C28	0.83313	0.52485	1.13556	
H29	0.67074	0.52182	0.66856	
H30	0.65555	0.58672	0.97420	
H31	0.61678	0.57992	0.44388	
H32	0.61618	0.29023	1.10028	
H33	0.55649	0.50636	0.33008	
H34	0.55578	0.22174	0.99486	

H35	0.67774	0.28113	0.93441
H36	0.50169	0.29696	0.95825
H37	0.44352	0.34670	0.41575
H38	0.74910	0.23349	1.57088
H39	0.73357	0.40837	1.63868
H40	0.41672	−0.07745	0.95741
H41	0.38877	0.21199	0.33265
H42	0.37603	−0.00446	0.59901
H43	0.78509	0.22433	1.08477
H44	0.46617	−0.02342	1.21369
H45	0.48953	0.12451	1.18386
H46	0.77497	0.58984	1.59210
H47	0.83767	0.33956	0.88829
H48	0.85582	0.57876	1.05182

Hydrogen-bond geometry (Å, º)

D—H···*A*	*D*—H	H···*A*	*D*···*A*	*D*—H···*A*
N4—H35···N7^{i}	1.05	1.86	2.906	174
N5—H36···O2^{ii}	1.03	1.91	2.923	168
N6—H45···O2^{ii}	1.02	2.03	3.034	166
C9—H29···O3^{iii}	1.10	2.39	3.482	170
C25—H43···O3^{i}	1.09	2.33	3.281	144
C26—H46···O1^{iv}	1.09	2.34	3.199	135

Symmetry codes: (i) −*x*+3/2, *y*−1/2, *z*−1/2; (ii) *x*, *y*, *z*+1; (iii) *x*, *y*, *z*−1; (iv) −*x*+3/2, *y*+1/2, *z*+1/2.